Journal of Molecular and Cellular Cardiology 141 (2020) 54–64

Contents lists available at ScienceDirect

Journal of Molecular and Cellular Cardiology

journal homepage: www.elsevier.com/locate/yjmcc

Original article

A cardiomyocyte show of force: A fluorescent alpha-actinin reporter line sheds light on human cardiomyocyte contractility *versus* substrate stiffness

Marcelo C. Ribeiro[a,1], Rolf H. Slaats[a,1], Verena Schwach[a], José M. Rivera-Arbelaez[a], Leon G.J. Tertoolen[b], Berend J. van Meer[b], Robert Molenaar[c], Christine L. Mummery[a,b], Mireille M.A.E. Claessens[c], Robert Passier[a,b,*]

[a] Department of Applied Stem Cell Technologies, TechMed Centre, University of Twente, Drienerlolaan 5, 7500AE Enschede, the Netherlands
[b] Department of Anatomy and Embryology, Leiden University Medical Centre, PO Box 9600, 2300, RC, Leiden, the Netherlands
[c] NanoBioPhysics Group, TechMed Centre, University of Twente, Drienerlolaan 5, 7500AE Enschede, the Netherlands

ARTICLE INFO

Keywords:
Transgenic model
Alpha-actinin
Contractility
Substrate stiffness

ABSTRACT

Cardiovascular disease is often associated with cardiac remodeling, including cardiac fibrosis, which may lead to increased stiffness of the heart wall. This stiffness in turn may cause subsequent failure of cardiac myocytes, however the response of these cells to increased substrate stiffness is largely unknown. To investigate the contractile response of human pluripotent stem cell-derived cardiomyocytes (hPSC-CMs) to increased substrate stiffness, we generated a stable transgenic human pluripotent stem cell line expressing a fusion protein of α-Actinin and fluorescent mRubyII in a previously characterized NKX2.5-GFP reporter line. Cardiomyocytes differentiated from this line were subjected to a substrate with stiffness ranging from 4 kPa to 101 kPa, while contraction of sarcomeres and bead displacement in the substrate were measured for each single cardiomyocyte. We found that sarcomere dynamics in hPSC-CMs on polyacrylamide gels of increasing stiffness are not affected above physiological levels (21 kPa), but that contractile force increases up to a stiffness of 90 kPa, at which cell shortening, deducted from bead displacement, is significantly reduced compared to physiological stiffness. We therefore hypothesize that this discrepancy may be the cause of intracellular stress that leads to hypertrophy and consequent heart failure *in vivo*.

1. Introduction

Disease of the heart often leads to remodeling of the heart wall, which can eventually lead to heart failure [1]. Cardiac remodeling is an adaptive response to heart function impairment. It is influenced by a variety of factors, including genetic predisposition, loss of viable cardiac tissue, volume- and pressure overload and myocarditis, among others. The most common features of cardiac remodeling are increased cardiomyocyte size, fibroblast proliferation and increased deposition of extracellular matrix (ECM) proteins. Together, these changes lead to increased cardiac wall stiffness, which is associated with (diastolic) heart failure [2–4]. Regardless of the underlying cause, cardiomyocytes increase their contraction force in response to increased stiffness, which may ultimately lead to adverse cardiac hypertrophy and cell death [5,6]. It is therefore important to determine how the cardiomyocyte adapts to an increase in stiffness and at which value the cell is not further able to contract, as this environment is a major stress trigger for adverse hypertrophy and cell death.

Sarcomeres are the smallest contractile units of cardiomyocytes. Sarcomeric organization, length and movement are key elements in the adaptability of cardiomyocyte contraction to increased stiffness. However, it is not clear how sarcomere length and movement are affected with increasing substrate stiffness in order to maintain cardiomyocyte contraction. Here, we generated a clonal transgenic *α-Actinin-mRubyII* fusion reporter using CRISPR-Cas9-mediated genome editing in a previously described cardiomyocyte fluorescent (*NKX2.5-eGFP*)

Abbreviations: ECM, extracellular matrix; hPSC-CM, human pluripotent stem cell-derived cardiomyocyte; PAA, polyacrylamide; hESC, human embryonic stem cell; bFGF, basic fibroblast growth factor; MEF, mouse embryonic fibroblasts; HDR, homology-directed repair; PDMS, polydimethylsiloxane; FACS, fluorescence-activated cell sorting; hIPSC, human induced pluripotent stem cell; CRISPR, Clustered Regularly Interspaced Short Palindromic Repeats

* Corresponding author at: Department of Applied Stem Cell Technologies, TechMed Centre, University of Twente, Drienerlolaan 5, 7500AE, Enschede, the Netherlands.
E-mail address: robert.passier@utwente.nl (R. Passier).
[1] Authors contributed equally to this work.

https://doi.org/10.1016/j.yjmcc.2020.03.008
Received 1 September 2019; Received in revised form 17 March 2020; Accepted 18 March 2020
Available online 20 March 2020

human pluripotent stem cell (hPSC) reporter line [7]. The resulting Double Reporter of *mRubyII-ACTN2* and *GFP-NKX2.5* (DRRAGN) line allows real-time monitoring of z-disk distance and contractile movement in live cardiomyocytes as substrate stiffness increases. Using the DRRAGN reporter line we assessed the adaptive response of contraction force of single hPSC-derived cardiomyocytes (hPSC-CMs) to increased substrate stiffness and measured sarcomere length and movement within the same cells. We found that different aspects of sarcomere dynamics of hPSC-CMs are differentially affected by increased substrate stiffness.

2. Methods

2.1. Plasmid design and construction

The Cas9 plasmid (Addgene #62988) carrying *CAS9* and the gRNA sequences was generated as described by Ran *et al* [8]. Briefly, gRNA-coding Fwd DNA oligonucleotide 5'-CACCGTTCTCTTCCGCACTCT ACG-3′ and Rev. DNA oligonucleotide 5'-AAACCGTAGAGTGCGGAAG AGAAC-3′ were ordered as single strand complementary DNA oligonucleotides (Sigma-Aldrich) and subsequently phosphorylated and annealed using T4 PNK (ThermoFisher) in a thermocycler running the parameters set by the protocol from Ran *et al.*, that creates sticky ends on the dsDNA fragment for seamless insertion into the plasmid. The annealed double stranded gRNA DNA oligo was then incorporated in the Cas9 plasmid by simultaneous cutting of the plasmid with restriction enzyme *BbsI* (ThermoFisher) and T7 (ThermoFisher) ligation of the oligo at the cut site. The Cas9 gRNA plasmid was then transformed and expanded in DH5a (ThermoFisher) bacteria and subsequently isolated and sent for Sanger sequencing (Eurofins Genomics) and stored for transfection.

The homology-directed repair template plasmid consisted of a pENTR1A backbone carrying the *mRubyII* sequence flanked by two homology arms of the target genomic locus of *ACTN2*, which would mediate homology-directed repair-based insertion of the *mRubyII* sequence into the host genome. The *mRubyII* sequence was amplified by hifi PCR (Phusion polymerase, ThermoFisher) using In-Fusion primers (mRubyII Fwd and Rev., see Suppl table 1) and plasmid mRubyII-N1 (Addgene #54614) as template. Homology arm sequences were amplified by hifi PCR of isolated human genomic DNA of HUVECs using In-Fusion primers (5′ flanking sequence Fwd and Rev. for the upstream homology arm, and 3′ flanking sequence Fed and Rev. for the downstream flanking sequence, see Suppl table 1). Using primers designed for In-Fusion cloning created overlapping termini after hifi PCR between each DNA fragment and the plasmid backbone at the insertion site that is required for In-Fusion based assembly of the HDR plasmid, as described in the Takara Clontech In-Fusion cloning manual. Care was taken to mutate the PAM sequence in the plasmid to prevent Cas9 from cutting the template plasmid during transfection (see Fig. 1C). To generate the targeting vector, amplified fragments were assembled by In-Fusion cloning (Takara CL 639648) according to the manufacturer's directions.

2.2. Stem cell maintenance

Human embryonic stem cells (hESCs, female) carrying a GFP reporter for NKX2.5 [7] were maintained on irradiated mouse embryonic fibroblasts (MEF feeder cells) in hESC medium (DMEM/F12-based medium containing 20% knockout serum replacement (ThermoFisher) and 10 ng/mL basic fibroblast growth factor (bFGF) (Miltenyi Biotech)). Passaging of hESCs on MEFs was done by dissociation using 1 × TripLE Select (ThermoFisher), subsequent inactivation by dilution in hESC medium, collection of the cells by centrifugation at 240 × *g* for three minutes, resuspension of the pellet in 1 mL hESC medium, manual counting using Trypan blue (ThermoFisher) and finally seeding as single cells on freshly prepared plates with MEF cells on 0.1% gelatin.

2.3. Transfection

HPSCs were maintained in hESC medium (see above) and were seeded at a density of 50 K cells per cm^2 on MEF cells one day before transfection. hPSCs were simultaneously transfected with 4 μg Cas9 plasmid and 2 μg of HDR plasmid using Lipofectamine 2000 (ThermoFisher) according to manufacturer's instructions. Transfected cells were selected by puromycin exposure for 72 h, followed by recovery culture on MEFs in hESC medium for seven days and passaged once to fresh feeder cells before single cell clonal expansion was initiated by flow cytometry-mediated single cell deposition onto MEF feeder cells in 96-well plates. Single cell colonies were manually identified and passaged to 48 well format on feeder cells. Insertion of the mRubyII sequence into one or both *ACTN2* alleles was validated by hifi PCR and subsequent gel electrophoresis. Two passages after single cell sorting and clonal expansion, the cells were transferred to vitronectin-coated plates without feeder cells and grown in Essential 8 medium (ThermoFisher).

2.4. Stem cell differentiation

Differentiation to cardiomyocytes was done as described previously [9]. Briefly, hPSCs were seeded at a density of 25 K cells per cm^2 on Matrigel-coated 6-well plates in Essential 8 medium (ThermoFisher) (described in [10]) on day −1. At day 0, mesodermal differentiation was initiated by addition of Wnt activator CHIR99021 (1.5 μmol/L, Axon Medchem 1386), Activin-A (20 ng/mL, Miltenyi 130–115-010) and BMP4 (20 ng/mL, R&D systems 314-BP/*CF*) in BPEL medium. At day 3, Wnt was inactivated by adding XAV939 (5 μmol/L, R&D Systems 3748) in BPEL. In addition, Matrigel (1:200) was added to promote adhesion of cells. Cell cultures were refreshed on Day 7 and 10 with BPEL after the start of differentiation until differentiation was completed (day 13).

2.5. Cell line validation

Proper insertion of the mRubyII sequence at the *ACTN2* locus was validated by Sanger sequencing (Eurofins Genomics) of Phusion hifi PCR (Thermofisher) products covering the insert within the HDR template and at the site of insertion in the genome of the targeted cells. Primers used for sequencing can be found in supplementary table 2. Human pluripotent stem cell identity was assessed by expression of TRA-1-60 (Miltenyi Biotech GmbH) quantified by MACSQuant VYB flow cytometer (Miltenyi Biotech GmbH). Potential off-target locations were identified using the Off-Spotter web tool of Jefferson.

2.6. Acrylamide gel fabrication

Coverslips of 15 mm diameter were micro-patterned with 1% gelatin lines (20 um width) using a PDMS stamp. Polyacrylamide (PAA) gels with varying degrees of stiffness were produced by mixing 40% acrylamide, HEPES (200 mM, pH 8.5), ammonium persulphate (10%) and H_2O (volume depending on Bis solution volume). This mixture was vortexed and spun down to remove air. Subsequently, TEMED and a 2% Bis solution at incrementing dilutions were added: 0.02%, 0.08%, 0.15%, 0.24%, 0.50% and 0.66%, and completed with 1 μL FluoSpheres, (Invitrogen, Ø 0.2 μm polystyrene beads loaded with dark red fluorophore Ex/Em = 660/680 nm). Precisely 9.2 μL of the polyacrylamide mixture was added at the center of a silane coated coverslip of 25 mm diameter to control thickness, then topped with micro-patterned coverslip before the acrylamide polymerized. Patterning coverslips were removed after 18 min of polymerization. Coverslips with patterned gels were UV sterilized before use. To measure gel stiffness, 5 circles of 1.5 mm thick PAA gels per stiffness with a diameter of 25 mm were compressed linearly in a wet state by a rheometer (Anton-Paar Physica MCR 301), which measured gap distance (remaining thickness

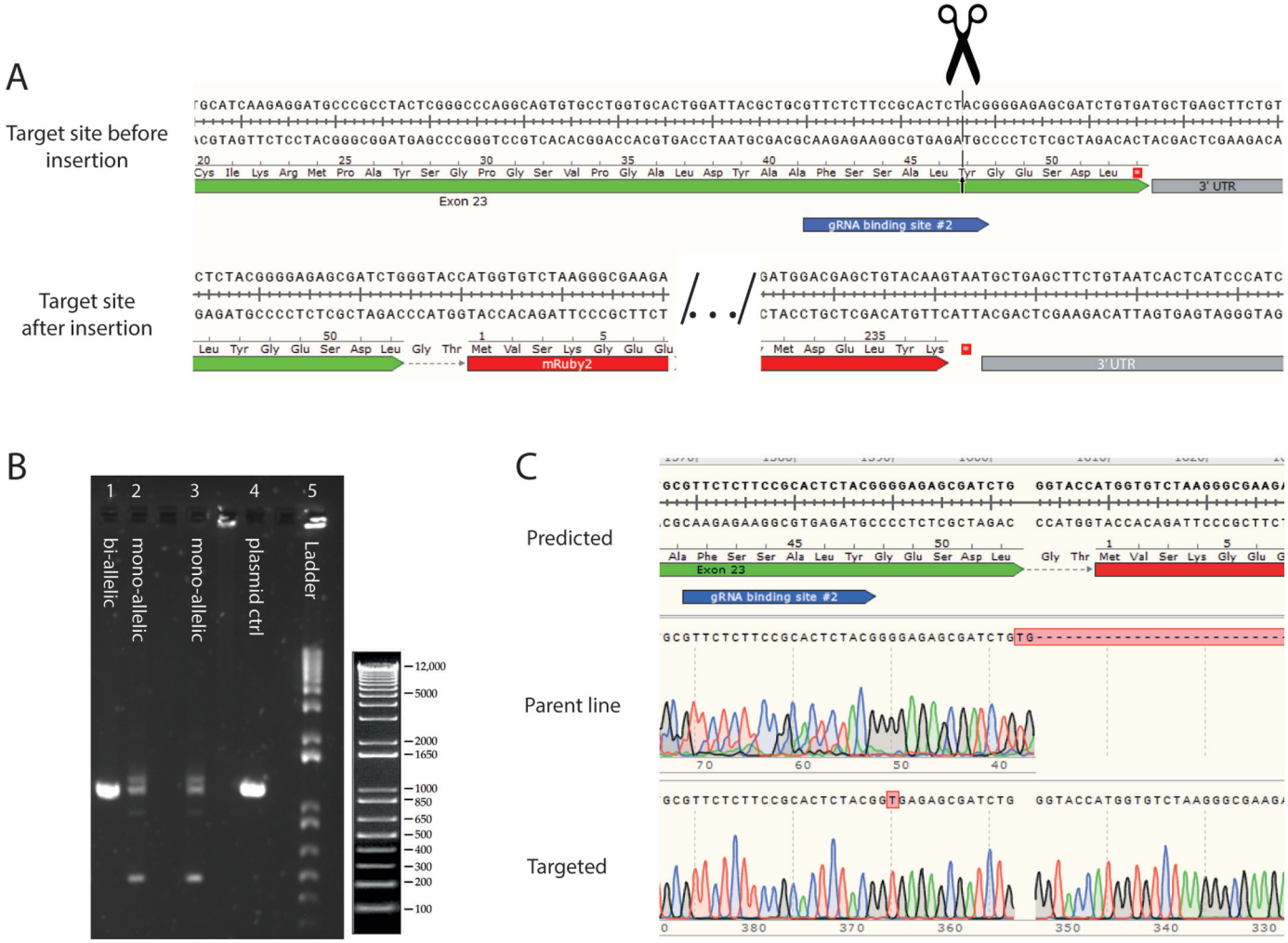

Fig. 1. The designed and validated targeting of the α-Actinin locus. A) The in-silico sequence of the α-Actinin locus before and after targeting. B) Agarose gel demonstrating mono-allelic and bi-allelic targeted α-Actinin loci. C) Sanger sequencing validation of the insert. Note the G- > T mutation in the targeted genome that corresponds with the PAM sequence inactivation in the construct.

of the gel, in mm) and the normal force (N) required to compress the gel to this thickness. We then used these readouts to approximate the Young's modulus of the gel using the following formula:

$$YM = \frac{dF/A}{dL/L_0}$$

where YM = Young's Modulus, dF = the increase in normal force from baseline to current compression, A = area of the plunger (=25 mm), dL/L_o = fraction of compression, with dL the gap distance at current compression compared to baseline L_0.

2.7. Cell culture on gels

HPSC-CMs were incubated in maturation medium [9] with a T3 hormone concentration of 5 μmol/L for three days starting at day 13 of the differentiation, followed by dissociation with 1× TripLE (ThermoFisher) and replating on the patterned coverslips at a density of 60 K cells per cm^2 on day 16. Cells were then allowed to recover for 4 days in maturation medium until start of image acquisition at day 20.

2.8. Data collection and analysis

HPSC-CMs seeded on gelatin patterns were maintained at 37 °C in 5% CO_2 during image analysis. Cardiomyocytes were paced at 1 Hz. Image acquisition was done at 70 frames per second for both bead displacement recording and α-Actinin tracking on a Nikon Eclipse TE2000-U fluorescence microscope fitted with a Nikon CFI Super Fluor 40× oil immersion objective (MRF01400) and a mercury light as excitation source. Alpha-Actinin-mRubyII was visualized at 60× magnification (using a 1.5× enhancer on the microscope) with filters at excitation 542/20 nm and emission 560LP; the fluorescent beads at 40× magnification using filters at excitation 620/60 and emission 700/75 nm. Transmitted light was captured at 40× magnification. The GFP signal was used to confirm individual cell identity as cells of the working myocardium, excluding cells of the nodal lineage during analysis. All data was collected from hPSC-CMs derived from one heterozygous (3F4) and one homozygous (3A1) clone (4 kPa: 58 and 44; 21 kPa: 43 and 44; 32 kPa: 33 and 48; 59 kPa: 49 and 46; 90 kPa: 43 and 45; 101 kPa: 27 and 44 cells for the heterozygous and homozygous clone, respectively) of at least 3 independent differentiations (n = 5 for 4 kPa group, n = 3 for other stiffnesses). Data was pooled and averaged across all cells of the same experimental group.

Bead displacement in the PAA gel was quantified using the Mosaic Particle Tracker plugin on ImageJ. The travel distances of all beads were calculated using the raw x and y coordinates of each particle in each frame. We exclusively analyzed moving beads that were located directly under the attached cardiomyocyte, using a tracing of the cell outline prepared manually for each cell on the transmitted light image. This outline was also used to determine cell area for normalization. Exerted stress (from here on referred to as force for ease of reading) of

the cell onto the substrate was calculated using the known substrate stiffness and the sum of travel distances of the beads, using a previously described Eq. [11], and normalized to cell area using the cell outline trace for fair comparison:

$$F_x = \frac{2}{(1+v)(2-v)} E_m b u$$

In which v = Poisson's ratio (= 0.457 for PAA [12]), b = bead diameter, u is displacement and E_m = Young's modulus, which is dependent on the stiffness of the gel. This equation assumes the beads are located at the surface of the gel for simplicity, which we took into account by focussing on the beads directly underneath the cell on the surface of the gel, using the 40× objective. The unit of measure for contraction force in this paper is μN/mm^2, whereas stiffness of the substrate is defined in kPa. These units of measure are interchangeable, but in order to facilitate comparison to literature we chose to report both forces in different units. For reference: 1 kPa = 1000 μN/mm^2.

To assess cell contraction distance (shortening), bead movement on the short edges of the cell was quantified. We identified these beads from the total bead population under the cell by selecting the 5% of beads showing greatest movement in the collected data.

Sarcomere kinetics were analyzed by custom made LabView-based software quantifying z-line movement using the fluorescent α-Actinin signal of the reporter cells (LabView, Vision and Motion, National Instruments Austin, Texas, USA). In short, eight individual *Z*-line profiles were recorded (for 8 to 10 contraction-relaxation cycles) per myofibril in the hPSC-CM (Suppl Fig. 8A). The profiles were analyzed by fast Fourier transformation which gave a central peak which was fitted (Levenberg-Marquardt algorithm) with a gaussian profile. The peak of the gaussian was taken for the computation of the amplitude at each point during the contraction relaxation amplitude (Suppl Fig. 8B). Contraction relaxation profiles were then computed plotting the amplitude (calibrated for μm/pixel) with the known time interval during recording. Beginning and end of contraction and relaxation were determined using this plotted contraction-relaxation profile based on changes in slope, after which the software calculated time and distance parameters of contraction and relaxation.

2.9. Statistics

Results are displayed as mean ± standard error of the mean (s.e.m.) unless stated otherwise. Statistical analyses were performed on IBM SPSS Statistics 25, comparing means of groups using one-way ANOVA and Bonferroni post-Hoc test.

3. Results

3.1. Characterization of the DRRAGN α-Actinin/NKX2.5 double reporter line

Incorporation of the DNA fragment (Suppl Fig. 1) encoding *mRubyII* at the genomic locus of *ACTN2* was facilitated by transfection of two vectors: A Cas9-gRNA plasmid and HDR template plasmid (Supply Fig. 2). The gRNA mediated DNA cleavage was directed 17 base pairs upstream of the stop codon at the end of the last exon of the *ACTN2* gene where the *mRubyII* sequence was inserted in frame *via* homology-directed repair. Of 192 single cells deposited by FACS after transfection and antibiotic selection, 82 colonies could be identified (survival of 43%), of which 22 clones were successfully targeted clones identified by PCR and subsequent gel electrophoresis. Fifteen of these were mono-allelic and 7 were bi-allelic (Fig. 1B). Sanger sequencing of these clones validated the insertion of the *mRubyII* sequence according to the *in silico* design (Fig. 1A + C). Of the 22 clones, three clones demonstrated a genetic alteration, of which one was a frame-shift mutation knocking out *mRubyII;* the other two were silent mutations (see suppl. Table 3). At this point, two sequence-validated mono-allelic (clone numbers 3A1 and 3A6) and two bi-allelic clones (numbers 4D2 and 3F4) were selected for further analysis. Off-target screening of these four clones revealed no mutations in the top 4 most likely targeted sites as predicted by the Off-Spotter web tool (Suppl Fig. 3). Targeted clonal lines revealed a high percentage (> 97%) of stem cell marker TRA-1-60 as shown by flow cytometry (Suppl Fig. 4).

3.2. Targeted hPSC cells differentiate efficiently to cardiomyocytes in vitro

Upon differentiation, the DRRAGN hPSC line to cardiomyocytes showed a clear and organized striated pattern of fluorescent α-Actinin along the long axis of the cell upon differentiation to cardiomyocytes, of which the homozygous clone expressed a higher average mRubyII signal intensity than the heterozygous clone as detected by flow cytometry (Fig. 2C). Fig. 2A shows the fluorescent signal of the α-Actinin under identical microscopic acquisition settings for both a mono-allelic (3A1) and a bi-allelic (3F4) clone, demonstrating that both genotypic variants were readily detectable. Compared to the parental cell line, all but mono-allelic clone 3A6 of the double reporter cell line differentiated into comparable percentages of cardiomyocytes [parental line 65.3 ± 3.2%; mono-allelic clones 3A1: 59.5 ± 4.0% & 3A6: 36.6 ± 4.5%; bi-allelic clones 4D2 63.5 ± 3.1% & 3F4 63.3 ± 2.7%], indicated by the *NKX2.5-GFP*$^+$ populations (Suppl Fig. 5+6). Interestingly, a subset of *NKX2.5*$^+$*/ACTN2*$^+$ (cardiomyocytes), *NKX2.5*$^+$*/ACTN2*$^-$, *NKX2.5*$^-$*/ACTN2*$^+$ and *NKX2.5*$^-$*/ACTN2*$^-$ populations could be identified in differentiated DRRAGN cultures following analysis by flow cytometry, which suggested cell populations were heterogeneous (Fig. 2B). Bi-allelic and mono-allelic clones showed similar population distributions except for 3A6, which had significantly ($p < .001$) fewer *NKX2.5-GFP*$^+$*/ACTN2-mRUBY*$^+$ cardiomyocytes, indicating less efficient cardiomyocyte differentiation.

3.3. Defined stiffness exposure of hPSC-CMs on gelatin patterned acrylamide gels

Several studies have reported physiological human adult cardiac wall stiffness to range from 24 kPa to 30 kPa, while patients suffering from congestive cardiomyopathy were reported to have cardiac wall stiffness over 100 kPa [13–15]. To model for heart wall stiffening, we increased the stiffness of the cardiomyocyte substrate using polyacrylamide gels with a stiffness ranging from 4 to 101 kPa (Fig. 3) and measured sarcomere shortening and contraction force. In order to decrease the cell-to-cell variability we aligned hPCS-CMs on 20 μm wide gelatin lines that were patterned on these acrylamide gels by microcontact printing (Fig. 3A). Adjustment of the PAA crosslinker concentration resulted in a near-linear increase of gel stiffness as measured by rheometry (Fig. 3B). The presence of evenly aligned gelatin patterns was verified microscopically for gels with all stiffnesses (Fig. 3C), on which hPSC-CMs were seeded. Single cardiomyocytes attached to the gelatin pattern were analyzed by real-time imaging of fluorescent beads in the acrylamide substrate and α-Actinin-mRubyII in the cell (Fig. 3D). We confirmed that the fusion of the mRubyII to the α-Actinin did not alter the contraction force of these cells in comparison to the cardiomyocytes from the parental stem cell line, using the substrate stiffness previously published for these cardiomyocytes (5.8 kPa) (Suppl. Fig. 7) [9].

3.4. hPSC-CMs increase their applied contraction force in response to increased substrate stiffness

HPSC-CMs displayed significantly increased contraction force as substrate stiffness increased up to 90 kPa ($p < .01$), above which the contraction force did not further increase (Fig. 4A). By tracking bead displacement on the contractile edges of the cardiomyocytes, we found that cell shortening was significantly higher at 4 kPa when compared to all the other stiffnesses ($p < .001$), indicating a significant change in

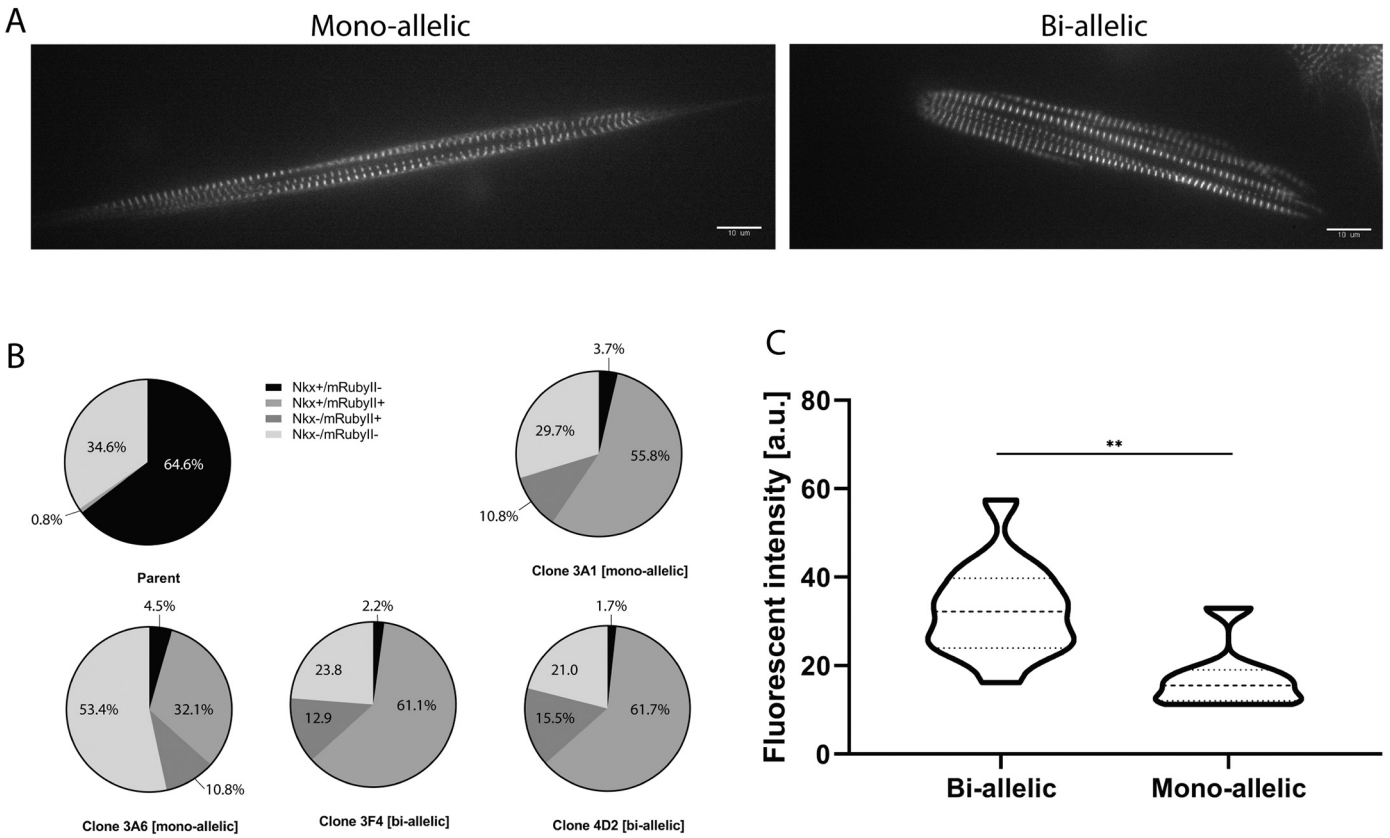

Fig. 2. DRRAGN hESC differentiate to cardiac cells, and specifically to cardiomyocytes, in a similar fashion to the parent line. A) Photomicrograph of a single cardiomyocyte expressing mono-allelic or bi-allelic fluorescent α-actinin after differentiation from the reporter cell line using identical acquisition settings. B) Populations of cells derived from monolayer differentiations ($n \geq 3$) of parent line (dN3), mono-allelic reporters (3A1 and 3A6) and bi-allelic reporters (3F4 and 4D2), with $NKX2.5^{+}/ACTN2^{+}$ population representing cardiomyocytes. C) Fluorescent signal intensity differs significantly ($p < .001$) between the homozygote clone 3F4 ($N = 14$) to heterozygote clone 3A1 ($N = 8$) as detected by flow cytometry. Significance: * = $p < .05$, ** = $p < .01$, *** = $p < .001$, ns = not significant.

cell response to its substrate between 4 kPa and the physiological-like 21 kPa stiffness. We observe a trend of decrease of cell shortening from 21 kPa and 90 kPa, whereas cell shortening significantly decreased at 101 kPa compared to the physiological-like 21 kPa stiffness ($p < .05$, Fig. 4B), indicating that this is the level of stiffness at which cell shortening is significantly restrained by the substrate. Neither the time of contraction nor relaxation changed significantly between the different stiffnesses (Fig. 4C), except the time of relaxation at 4 kPa, which was significantly lower than the time at 21 kPa (424 ± 19 *vs* 520 ± 29 ms, $p < .05$). However, the speed of contraction and relaxation decreased significantly from 4 kPa to 21 kPa and to the higher stiffnesses. Both speed of contraction and relaxation gradually decreased from 21 kPa and higher stiffnesses, with a significant change at 101 kPa (Fig. 4D).

3.5. Sarcomeric shortening does not change at supraphysiological substrate stiffnesses

Sarcomeric movement was measured on the same cardiomyocytes as in bead displacement measurement in Fig. 4 (Suppl video 1). Substrate stiffness appeared not to affect sarcomeric organization of cardiomyocytes (Fig. 5A), except for the lowest stiffness of 4 kPa, on which the cardiomyocytes retained a more elliptic morphology compared to other stiffnesses. The sarcomere length (spacing between two z-disks) of 1.54 ± 0.014 μm at maximum contraction did not significantly change with the increase in substrate stiffness except between 4 kPa and 32 kPa ($p < .05$), and sarcomere length at full relaxation remained constant around 1.73 ± 0.015 μm (Fig. 5B), except at 4 kPa, where sarcomere length was on average 1.85 ± 0.02 μm ($p < .001$). The shortening of the sarcomere (measured in z-disk displacement) significantly decreased from 0.34 ± 0.014 μm at 4 kPa to 0.21 ± 0.01 μm at the physiological-like 21 kPa ($p < .001$) and remained constant with further increase in substrate stiffness (Fig. 5C), indicating that the sarcomere shortening does not adapt to increase in substrate stiffness beyond physiological-like stiffnesses. Even though the duration of both sarcomere contraction (210 ± 1.1 ms) and relaxation (300 ± 1.8 ms) did not change with the increase in substrate stiffness (Fig. 5D), both sarcomere contraction and relaxation speed significantly decreased from 4 kPa up to 32 kPa ($p < .001$) and remained constant with the further increase in substrate stiffness (Fig. 5E), which reiterates the sarcomere maximum adjustment up to a substrate stiffness between 21 and 32 kPa. No differences in sarcomeric dynamics were observed between the mono-allelic and bi-allelic clone (Suppl. Fig. 9).

3.6. Adaptation of sarcomere contraction diverges from cell contraction at higher substrate stiffnesses

We measured both contraction force and sarcomere shortening in the same cells in order to assess the correlation of these two parameters with the increase in substrate stiffness. Interestingly, both sarcomere shortening and bead displacement during contraction significantly decreased from a very soft substrate to a more physiological substrate. However, at higher stiffnesses the bead displacement significantly decreased while sarcomere shortening and elongation were maintained (Fig. 6A, statistics in 4B & 5C), implying a decoupling between the sarcomere shortening and actual cell shortening capacity. Furthermore,

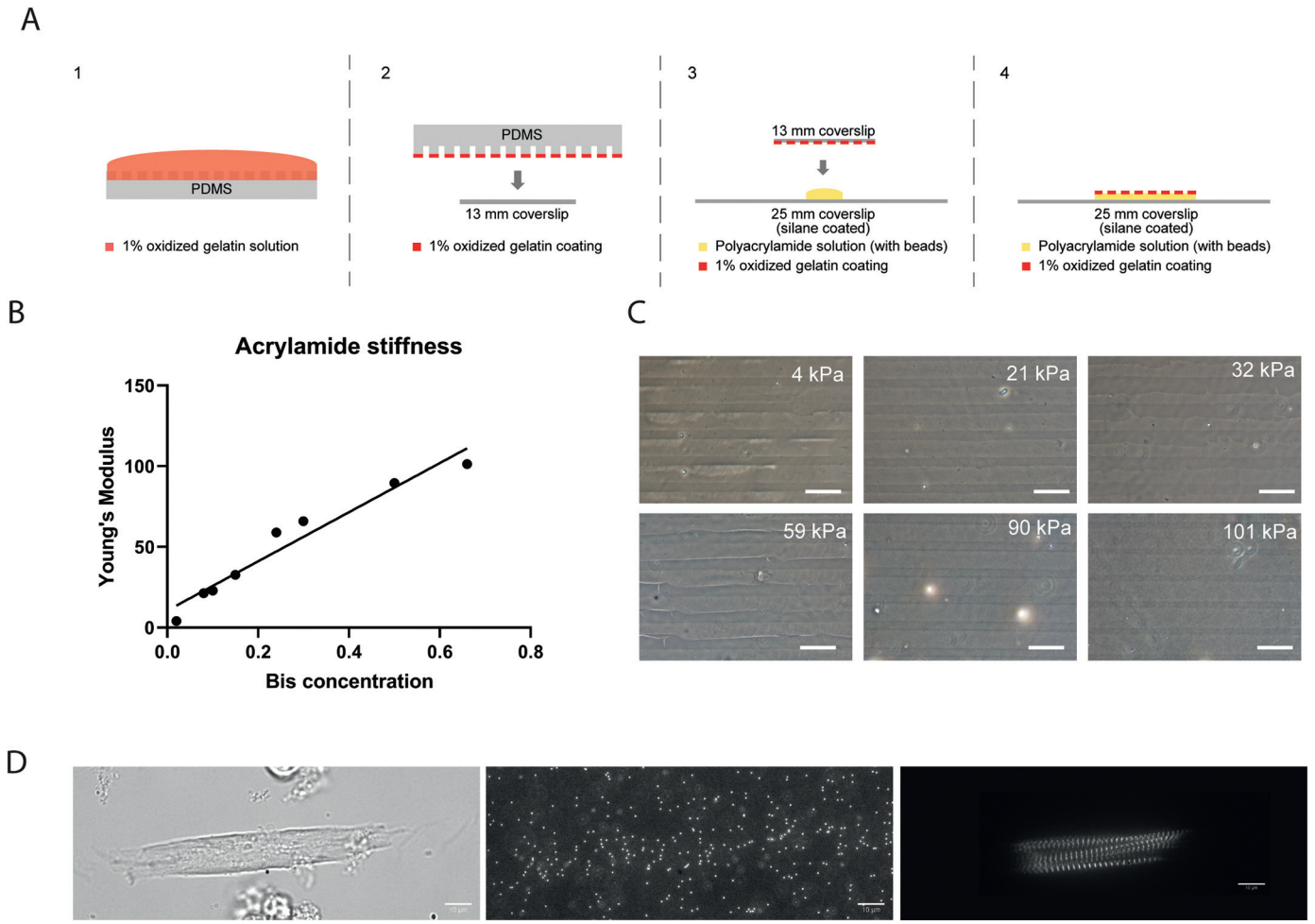

Fig. 3. The manufacturing of substrates with defined stiffness and single cardiomyocyte attachment. A) Schematic representation of micro-contact printing gelatin line patterns on PAA gels. B) Increased crosslinker in the PAA mixture provides gels with increasing Young's Modulus (stiffness). C) Photomicrographic representations of gelatin lines on acrylamide gels ranging from 4 kPa to 101 kPa in Young's Modulus. Scale bars represent 20 μm. D) A single cardiomyocyte attached to a gelatin line, imaged in transmitted light microscopy (left), the underlying fluorescent beads in the PAA gel (middle), and the corresponding α-Actinin signal of the cell (right). Scale bars represent 10 μm.

we observed that although sarcomere shortening was maintained through higher stiffnesses, the contraction force applied by the cell reached its limit around the 90 kPa substrate stiffness (Fig. 6B), indicating that the maximum force that the sarcomeres of these cells can generate is around 160 ± 14 μN/mm^2. This is corroborated by the fact that at a higher substrate stiffness (101 kPa) both the bead displacement (cell shortening) is significantly smaller and the contraction force reaches a plateau (Fig. 6C). Finally, we observed that time to contract and relax of hPSC-CMs based on bead displacement is more than 2-fold higher than the time required for combined sarcomeric contraction and relaxation. This observed difference was maintained with the increase in substrate stiffness (Fig. 6D). This discrepancy suggests that transfer of sarcomeric to cellular movement may be delayed by a stretch or relative movement of the adhesion complexes at the adhesion points of the cell to the gel.

4. Discussion

In this study we generated an α-Actinin/NKX2.5 double reporter line (DRRAGN), which allowed live imaging of sarcomeric organization and dynamics specifically in cardiomyocytes of the working myocardium, differentiated from hPSCs, and enabled evaluation of both sarcomere shortening and contraction force in the same hPSC-CMs at increasing levels of substrate stiffness. We found that force generation increased up to 90 kPa but cardiomyocyte shortening gradually decreased. Moreover, sarcomere shortening decreased up to physiological substrate stiffness (21 kPa), but remained constant thereafter. By assessing both of these parameters in each cell we could show that sarcomere shortening did not correlate with cell shortening, and consequently with contraction force output, at stiffness higher than 90 kPa.

Increased myocardial wall stiffness through cardiac remodeling is a response to impaired heart function and may ultimately lead to end-stage heart failure. The use of a hPSC sarcomeric reporter line allows for the assessment of contraction force and sarcomere function within the same single hPSC-CM, in response to increased substrate stiffness. Stable endogenous expression of fluorescently tagged α-Actinin has the advantage over previously reported lentiviral transduced constructs of uniform expression of α-Actinin-mRubyII across all single cardiomyocytes in culture [16,17]. Moreover, due to the double nature of our reporter for NKX2.5 and α-Actinin, the DRRAGN line can also be used to study early stages of differentiation towards cardiac cells, as well as in the identification or separation of cardiac subpopulations. For example, sinoatrial pacemaker or nodal cells of the heart, which have been reported to lack expression of NKX2.5, leaving them single positive for α-Actinin-mRubyII expression [18].

Analysis of contraction force of single aligned cardiomyocytes cultured on a substrate with different stiffnesses showed their capacity to adapt to the increase in stiffness by increasing contractile force output

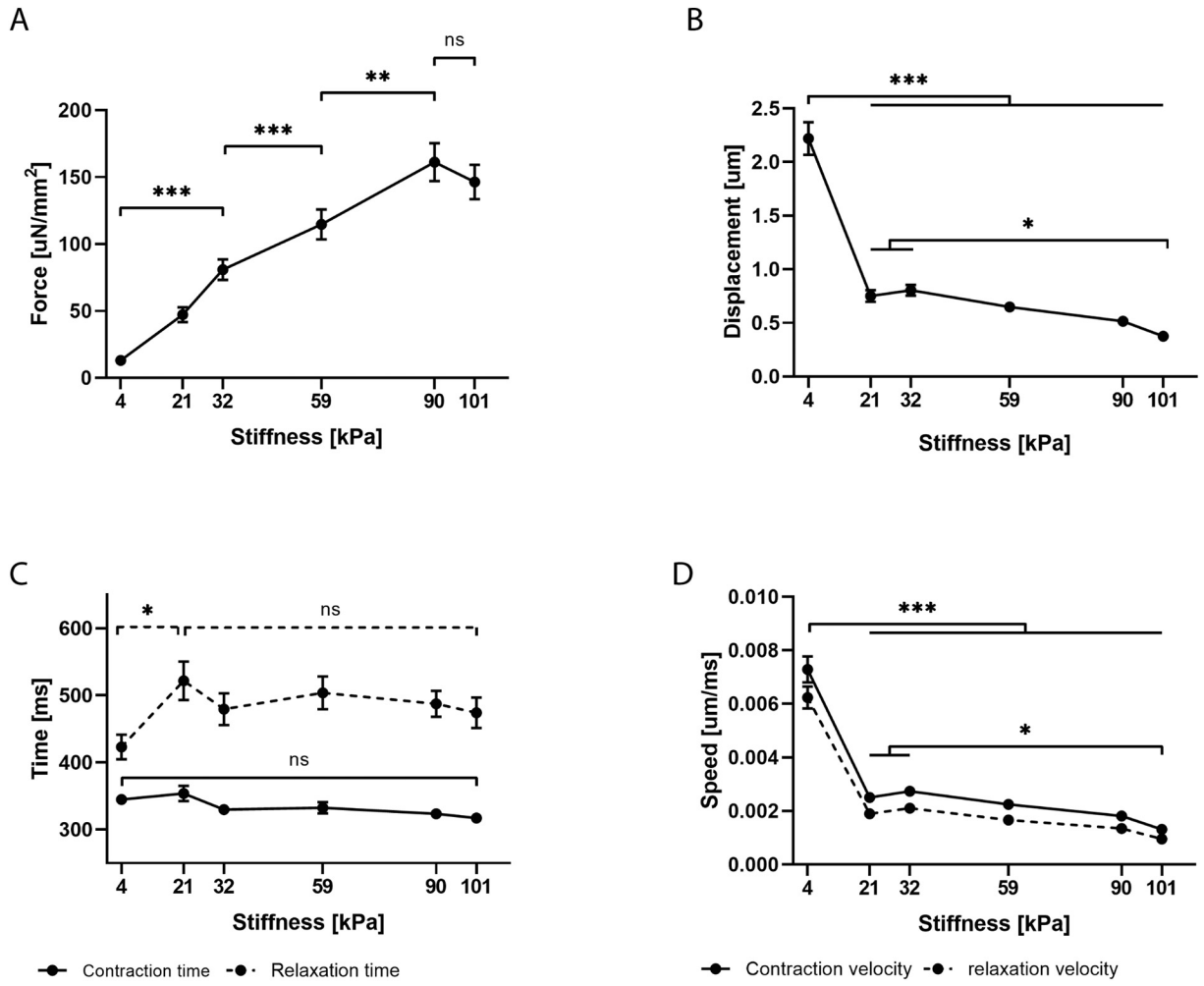

Fig. 4. Quantification of the manipulation of the PAA substrate by the cardiomyocytes (pooled data from heterozygous and homozygous clone). A) Average applied force on the acrylamide gel by the cardiomyocyte per substrate stiffness, normalized to cell surface area B) Average length of bead travel trajectory in the PAA gel upon contraction of the cardiomyocyte. C) Average time of substrate shrinkage and elongation due to cardiomyocyte contraction and relaxation, respectively. D) The average speed of contraction and relaxation as a function of bead travel time and displacement. Data presented in mean ± s.e.m. Significance: * = $p < .05$, ** = $p < .01$, *** = $p < .001$, ns = not significant. (n = 104, 99, 96, 102, 94 and 98 cells for groups 4 kPa, 21 kPa, 32 kPa, 59 kPa, 90 kPa and 101 kPa, respectively).

up to 90 kPa, which is in agreement with previous descriptions using human induced pluripotent stem cell- (hiPSC-), hESC- and rat-derived cardiomyocytes by Hazeltine *et al* [19]. Interestingly, we showed for the first time that single hPSC-CMs are able to maximally generate a force of 160 ± 14 μN/mm^2, as this value was maintained on substrates from 90 kPa to 101 kPa stiffness. However, hPSC-CMs generate less force than their maximum capacity when maximum force is not required (lower substrate load reduced the required and thus generated force by the cardiomyocytes). This means that hPSC-CMs reach their maximum contraction force capacity at substrate stiffness of 90 kPa. These results are in accordance with diseases such as congestive cardiomyopathy where cardiac wall stiffness is well above 100 kPa [2], leading to heart failure and ultimately cardiac death as the heart becomes unable to cope with the increasing load (contraction resistance) generated by the high stiffness of its walls.

The force applied on the 4 kPa stiff gels was significantly lower than other substrate stiffnesses, while bead movement was significantly larger, meaning that the cell applies a relatively low force for maximal shortening. The most pronounced adaptation of hPSC-CMs occurred between 4 kPa and physiological-like 21–30 kPa, as both bead displacement (cell shortening) and sarcomere shortening, as well as corresponding speeds, significantly decreased over this range. This effect is a response to the increase in load applied by the substrate to the cell. As described by Engler et al. 2008, at lower stiffness the cardiomyocytes do not produce maximal force output due to the low opposing load of the substrate, while at physiological stiffness, the opposing load of the substrate is optimal for the cardiomyocyte to generate maximum contractile work [20]. Our results show that the increase in substrate stiffness from 4 kPa to 21–32 kPa induces a sarcomeric adjustment to both decreased contraction and elongation (increased sarcomere length at full contraction and decrease sarcomere length at full relaxation), which is translated to a decreased sarcomere shortening during contraction and consequently a decreased cell shortening distance. Interestingly, at higher stiffnesses this sarcomere length adjustment does not occur but the cell shortening distance continues to decrease, which suggests that at higher stiffnesses the cell is spending more energy to generate more force as the opposing load of the substrate restrains the cell from shortening maximally, in similarity to the increase in energetic cost of contraction in patients with hypertrophied hearts [21]. *In vivo,* this increase in stiffness beyond the healthy physiological range has the consequence of higher energy spending during isometric systole phase in order to increase intraventricular pressure and transition to the ejection phase, which at very high wall stiffnesses likely translates to lower ventricle compression capability and lower stroke volume (Fig. 7). Such cardiac energy inefficiency has been described in patients with systolic dysfunction and associated with development and

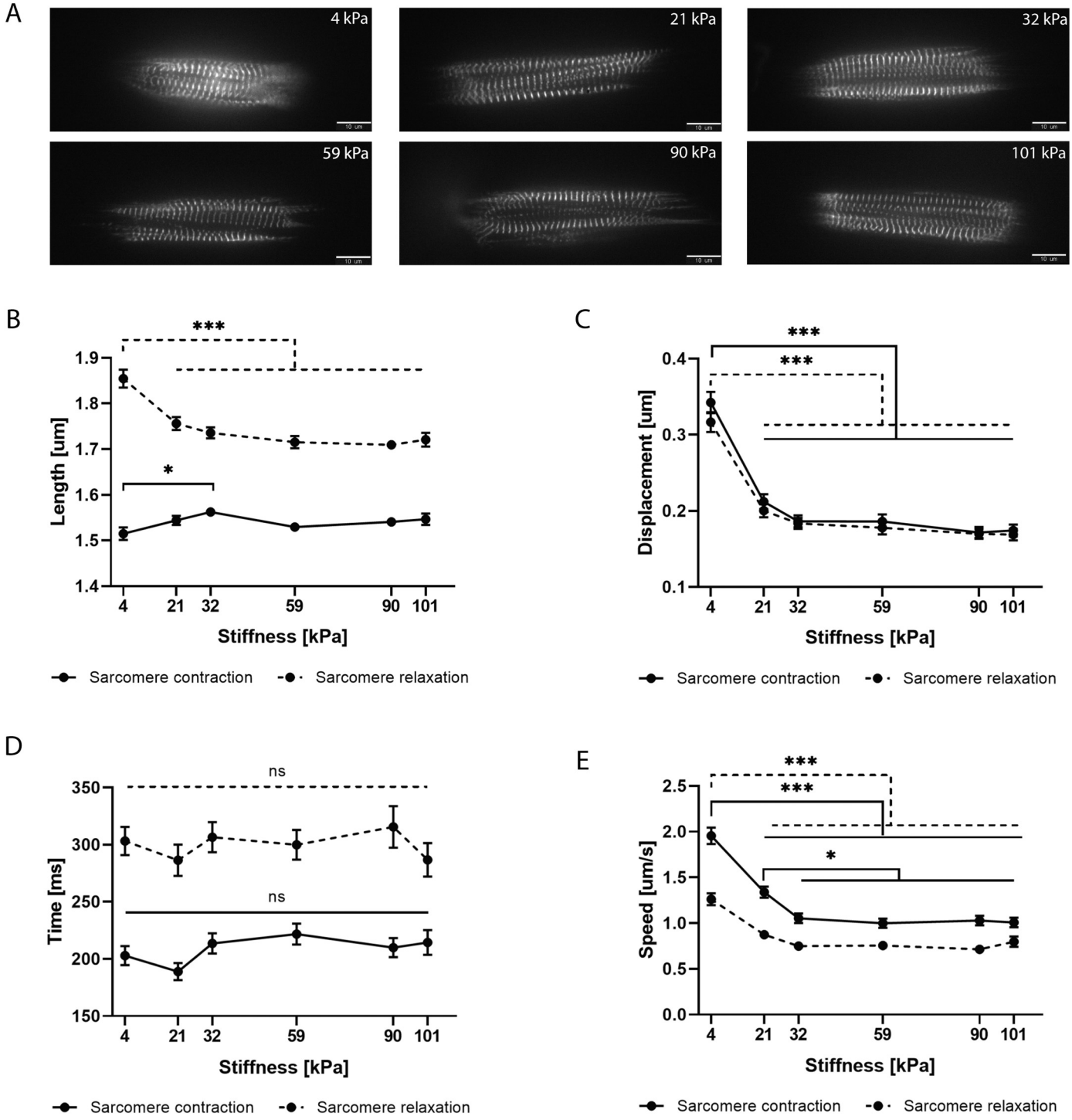

Fig. 5. Sarcomeric dynamics in relation to substrate stiffness (pooled data from heterozygous and homozygous clone). A) Representative pictures of single cardiomyocytes attached to gelatin on all different PAA stiffness. B) The absolute maximum and minimum length of the space between two z-disks (a sarcomere) at full relaxation and full contraction, respectively. C) The absolute shortening and elongation of the space between two z-disks during contraction and relaxation, respectively. D) Travel time of the z-disk (α-actinin line) during contraction and relaxation of the sarcomere. E) The travel speed of the z-disk line during contraction and relaxation. Data presented in mean ± s.e.m. Significance: * = p < .05, ** = p < .01, *** = p < .001, ns = not significant. (n = 102, 87, 81, 95, 87 and 71 cells for groups 4 kPa, 21 kPa, 32 kPa, 59 kPa, 90 kPa and 101 kPa, respectively).

progression of diastolic heart failure [22,23].

Furthermore, different studies have shown that cardiomyocytes are able to "sense" their surroundings and to respond to biomechanical cues [5,24]. Our results show that at substrate stiffness higher than 90 kPa, cardiomyocytes shorten significantly less while sarcomere shortening is maintained. These observations suggest that the force generated by the sarcomere contraction is applied to, and partially absorbed by, stretching of internal cytoskeletal filaments that connect the sarcomeres to the focal adhesions and desmosomes (Fig. 7). *In vivo* restraint of cardiomyocyte shortening by such increased wall stiffness has the effect of decreasing stroke volume, leading to a decreased cardiac output. One of the possible responses of cardiomyocytes to counter this restrain is to build more contractile sarcomere myofilaments in order to overcome the opposing load imposed by the high wall stiffness, which by

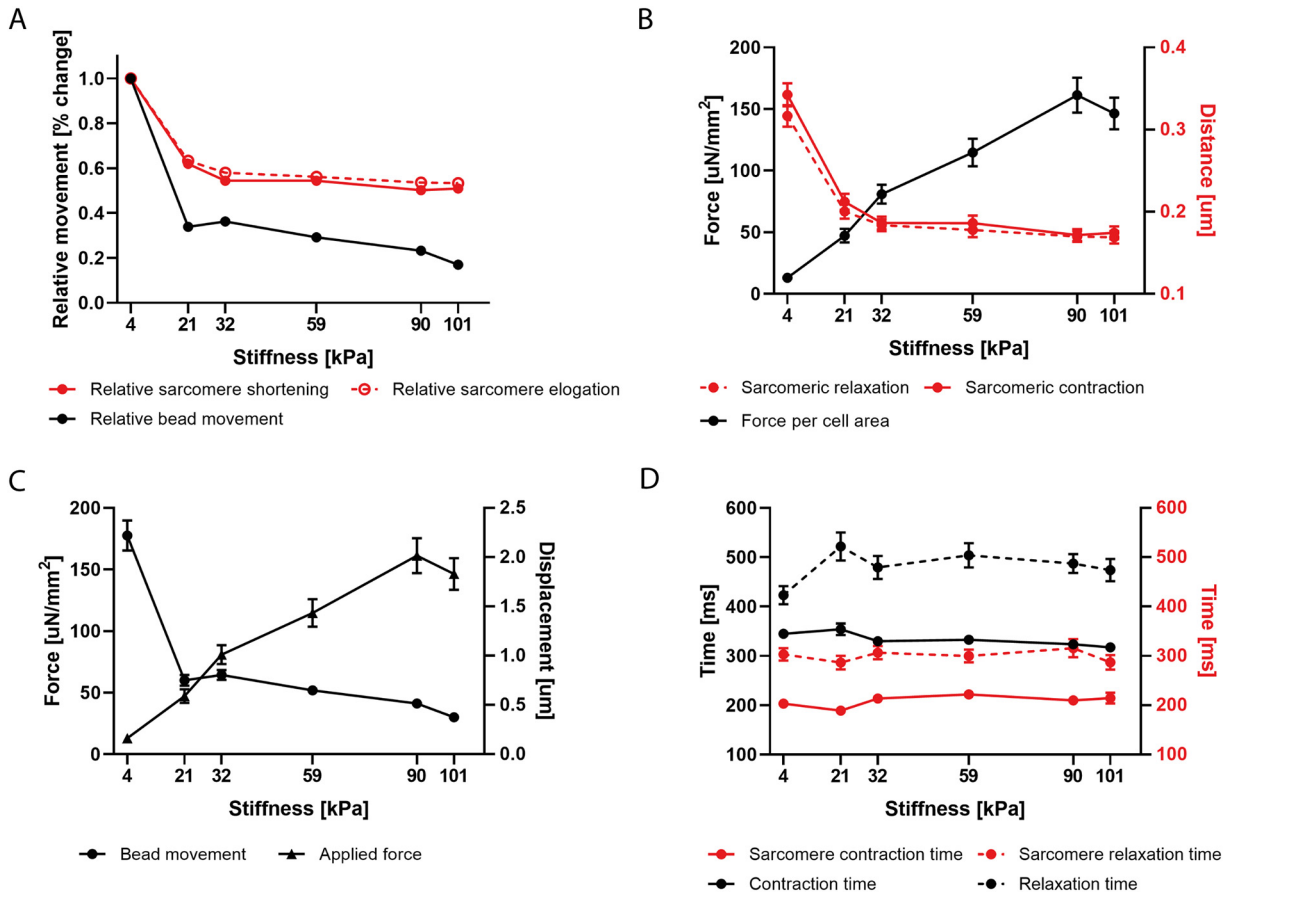

Fig. 6. Correlations between sarcomere dynamics data and substrate displacement quantification. A) In contrast to sarcomere shortening (in red), bead displacement continues to drop with increasing stiffness. B) Increase of force generated by the cardiomyocytes at higher stiffness is not explained by changes in sarcomere shortening (in red). C) As maximum force of the cardiomyocyte is reached at 90 kPa, cell shortening is significantly reduced upon further increase in stiffness of substrate. D) Both sarcomere (in red) and bead contraction and relaxation time are unaffected by substrate stiffness. Note that cell contraction in general takes longer than sarcomere contraction. Data presented in mean ± s.e.m. (For interpretation of the references to color in this figure legend, the reader is referred to the web version of this article.)

definition further increases the wall stiffness [25]. Such a self-propagating cycle has been shown to be the major biomechanical stress in the development and progression of cardiac diseases such as dilated and hypertrophic cardiomyopathies and heart failure [5,26,27]. Our *in vitro* model for adaptation of sarcomere dynamics with variable substrate stiffness provides a first basis to model this aspect of heart failure. We establish a variable substrate stiffness with a clear readout on the sarcomere dynamics that can be further coupled with coculture of CMs with fibroblasts, sarcomere mutations and analysis on metabolic derangements and on calcium handling in order to investigate heart failure in a more comprehensive manner.

5. Conclusion

We generated a stable transgenic hPSC reporter line that expresses fluorescent α-Actinin-mRubyII upon differentiation to cardiomyocytes, which enabled us to mimic and model “cardiac wall stiffening” *in vitro*. With this model we showed that increasing substrate stiffness affected cardiomyocyte contractile behavior of both sarcomere shortening and force generation. We conclude that the maximal sarcomere length adaptation to increased stiffness is reached in the physiological range of 21–32 kPa, while the contraction force generated keeps rising until reaching its maximum at 90 kPa. Finally, the discrepancy between sarcomere shortening and the magnitude of cell shortening at stiffnesses higher than 90 kPa suggests a “tipping” point at which stress-induced mechanisms are activated in cardiomyocytes. Here, we show an *in vitro* model which enables studying the underlying mechanisms of cardiac remodeling and heart failure at the cardiomyocyte level.

Acknowledgments

We thank Kim Vermeul and Simone ten Den for their continuous technical support during the experiments leading up to this paper, and B. Blankevoort for the illustration design.

Sources of funding

M.C.R. is supported by ZonMW MKMD-114022507, V.S. by ERA-CVD 2016T092 and the Dutch Heart Foundation, R.P., C.L.M., J.M.-R-A. by the NWO Gravitation project (024.003.001).

Disclosures

RP is co-founder of Ncardia and River BioMedics. MCR is co-founder of River BioMedics.

Data availability

The raw/processed data required to reproduce these findings cannot be shared at this time due to technical or time limitations.

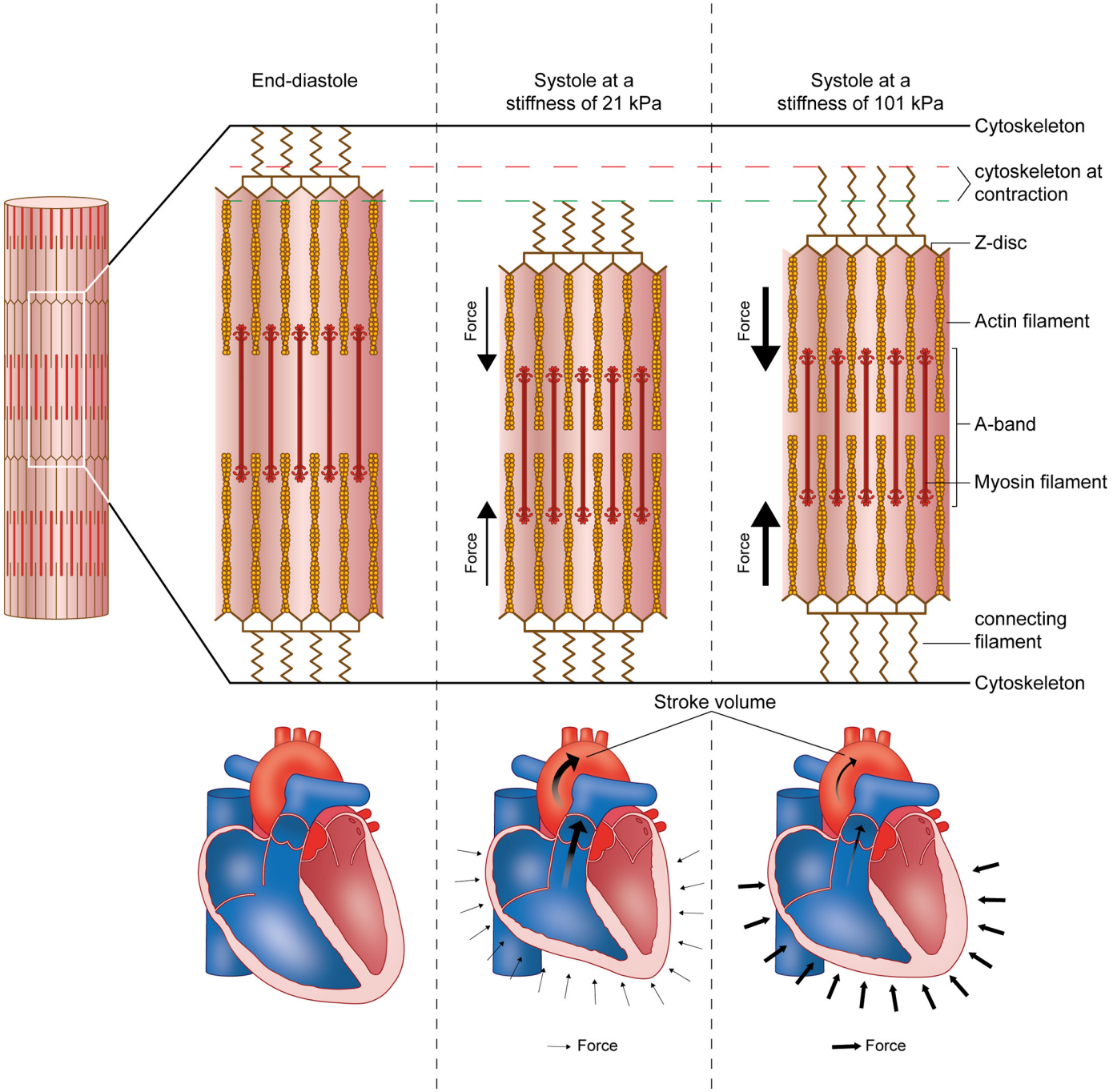

Fig. 7. Schematic representation of a possible change in contractile behavior with increase in substrate stiffness. Left, the representation of a myofibril with sarcomeres connected in series. Center-top: When the cell contracts from end-diastole to end-systole the sarcomere shortens pulling the cytoskeleton and the adhesion proteins with it. At substrate stiffness of 21 kPa the cytoskeleton and adhesion proteins are relatively free to move with the sarcomere shortening generated with a relatively low force, which *in vivo* can be translated into a large compression of the ventricle wall and consequent normal stroke volume (center-bottom). When the substrate stiffness increases to 101 kPa or higher the cytoskeleton and adhesion proteins are restrained by the substrate from moving freely with the sarcomere shortening although the force generated has significantly increased. In the working myocardium *in vivo* cardiomyocytes have to generate an increasing amount of force, in order to increase intraventricular pressure and transition from isometric systole phase to ejection phase. At very high wall stiffnesses, this may translate to lower ventricle compression, despite the larger force applied by the cells, and consequently may lead to a reduction in stroke volume.

Appendix A. Supplementary data

Supplementary data to this article can be found online at https://doi.org/10.1016/j.yjmcc.2020.03.008.

References

[1] J.N. Cohn, R. Ferrari, N. Sharpe, Cardiac remodeling—concepts and clinical implications: a consensus paper from an international forum on cardiac remodeling, J. Am. Coll. Cardiol. 35 (3) (2000 Mar 1) 569–582.

[2] R.R. Chaturvedi, T. Herron, R. Simmons, D. Shore, P. Kumar, B. Sethia, et al., Passive stiffness of myocardium from congenital heart disease and implications for diastole, Circulation. 121 (8) (2010 Mar 2) 979–988.

[3] A.S. Bortone, O.M. Hess, A. Chiddo, A. Gaglione, N. Locuratolo, G. Caruso, et al., Functional and structural abnormalities in patients with dilated cardiomyopathy, J. Am. Coll. Cardiol. 14 (3) (1989 Sep 1) 613–623.

[4] M.R. Zile, C.F. Baicu, S. Ikonomidis J, Stroud RE, Nietert PJ, Bradshaw AD, et al., Myocardial stiffness in patients with heart failure and a preserved ejection fraction,

Circulation. 131 (14) (2015 Apr 7) 1247–1259.
[5] P. Pandey, W. Hawkes, J. Hu, W.V. Megone, J. Gautrot, N. Anilkumar, et al., Cardiomyocytes sense matrix rigidity through a combination of muscle and non-muscle myosin contractions, Dev. Cell 44 (3) (2018 Feb 5) 326–336 e3.
[6] A. Piek, R.A. de Boer, H.H.W. Silljé, The fibrosis-cell death axis in heart failure, Heart Fail. Rev. 21 (2) (2016 Mar 16) 199–211.
[7] D.A. Elliott, S.R. Braam, K. Koutsis, E.S. Ng, R. Jenny, E.L. Lagerqvist, et al., NKX2-5 eGFP/w hESCs for isolation of human cardiac progenitors and cardiomyocytes, Nat. Methods 8 (12) (2011 Dec 23) 1037–1040.
[8] F.A. Ran, Hsu PDPPD, Wright J, Agarwala V, Scott D a, Zhang F. genome engineering using the CRISPR-Cas9 system, Nat. Protoc. 8 (11) (2013) 2281–2308.
[9] M.J. Birket, M.C. Ribeiro, G. Kosmidis, D. Ward, A.R. Leitoguinho, V. van de Pol, et al., Contractile defect caused by mutation in MYBPC3 revealed under conditions optimized for human PSC-Cardiomyocyte function, Cell Rep. 13 (4) (2015 Oct 27) 733–745.
[10] E.S. Ng, R. Davis, E.G. Stanley, A.G. Elefanty, A protocol describing the use of a recombinant protein-based, animal product-free medium (APEL) for human embryonic stem cell differentiation as spin embryoid bodies, Nat. Protoc. 3 (5) (2008 May 1) 768–776.
[11] M.L. McCain, H. Yuan, F.S. Pasqualini, P.H. Campbell, K.K. Parker, Matrix elasticity regulates the optimal cardiac myocyte shape for contractility, Am. J. Physiol. Heart Circ. Physiol. 306 (11) (2014 Jun 1) H1525–H1539.
[12] T. Takigawa, Y. Morino, K. Urayama, T. Masuda, Poisson's ratio of polyacrylamide (PAAm) gels, Polym Gels Networks. 4 (1) (1996 Jan 1) 1–5.
[13] I. Mirsky, W.W. Parmley, Assessment of passive elastic stiffness for isolated heart muscle and the intact heart, Circ. Res. 33 (2) (1973 Aug) 233–243.
[14] A. Borbély, J. van der Velden, Z. Papp, J.G.F. Bronzwaer, I. Edes, G.J.M. Stienen, et al., Cardiomyocyte stiffness in diastolic heart failure, Circulation. 111 (6) (2005 Feb 15) 774–781.
[15] H. Kanai, Propagation of spontaneously actuated pulsive vibration in human heart wall and in vivo viscoelasticity estimation, IEEE Trans. Ultrason. Ferroelectr. Freq. Control 52 (11) (2005 Nov) 1931–1942.
[16] C.N. Toepfer, A. Sharma, M. Cicconet, A.C. Garfinkel, M. Mücke, M. Neyazi, et al., SarcTrack: an adaptable software tool for efficient large-scale analysis of sarcomere function in hipsc-cardiomyocytes, Circ. Res. 124 (8) (2019 Jan 31) 1172–1183 CIRCRESAHA.118.314505.
[17] A. Mathur, P. Loskill, K. Shao, N. Huebsch, S. Hong, S.G. Marcus, et al., Human iPSC-based cardiac microphysiological system for drug screening applications, Sci. Rep. 5 (2015) 8883.
[18] A. Sizarov, H.D. Devalla, R.H. Anderson, R. Passier, V.M. Christoffels, A.F.M. Moorman, Molecular analysis of patterning of conduction tissues in the developing human heart, Circ. Arrhythm. Electrophysiol. 4 (4) (2011 Aug) 532–542.
[19] L.B. Hazeltine, C.S. Simmons, M.R. Salick, X. Lian, M.G. Badur, W. Han, et al., Effects of substrate mechanics on contractility of Cardiomyocytes generated from human pluripotent stem cells, Int J Cell Biol. 2012 (2012 May 9) 1–13.
[20] A.J. Engler, C. Carag-Krieger, C.P. Johnson, M. Raab, H.-Y. Tang, D.W. Speicher, et al., Embryonic cardiomyocytes beat best on a matrix with heart-like elasticity: scar-like rigidity inhibits beating, J. Cell Sci. 121 (22) (2008 Nov 15) 3794–3802.
[21] E.R. Witjas-Paalberends, A. Güçlü, T. Germans, P. Knaapen, H.J. Harms, A.M.C. Vermeer, et al., Gene-specific increase in the energetic cost of contraction in hypertrophic cardiomyopathy caused by thick filament mutations, Cardiovasc. Res. 103 (2) (2014 Jul 15) 248–257.
[22] S. HASEGAWA, K. YAMAMOTO, Y. SAKATA, Y. TAKEDA, K. KAJIMOTO, Y. KANAI, et al., Effects of cardiac energy efficiency in diastolic heart failure: assessment with positron emission tomography with 11C-acetate, Hypertens. Res. 31 (6) (2008 Jun 1) 1157–1162.
[23] F.M. Bengel, B. Permanetter, M. Ungerer, S. Nekolla, M. Schwaiger, Non-invasive estimation of myocardial efficiency using positron emission tomography and carbon-11 acetate–comparison between the normal and failing human heart, Eur. J. Nucl. Med. 27 (3) (2000 Mar) 319–326.
[24] R.C. Lyon, F. Zanella, J.H. Omens, F. Sheikh, Mechanotransduction in cardiac hypertrophy and failure, Circ. Res. 116 (8) (2015 Apr 10) 1462–1476.
[25] W. Grossman, W.J. Paulus, Myocardial stress and hypertrophy: a complex interface between biophysics and cardiac remodeling, J. Clin. Invest. 123 (9) (2013 Sep) 3701–3703.
[26] F. Sheikh, A. Raskin, P.-H. Chu, S. Lange, A.A. Domenighetti, M. Zheng, et al., An FHL1-containing complex within the cardiomyocyte sarcomere mediates hypertrophic biomechanical stress responses in mice, J. Clin. Invest. 118 (12) (2008 Dec 1) 3870–3880.
[27] G.Y. Oudit, Z. Kassiri, J. Zhou, Q.C. Liu, P.P. Liu, P.H. Backx, et al., Loss of PTEN attenuates the development of pathological hypertrophy and heart failure in response to biomechanical stress, Cardiovasc. Res. 78 (3) (2008 Jan 24) 505–514.